Silicon (2022) 14:4955–4967
https://doi.org/10.1007/s12633-021-01289-9

ORIGINAL PAPER

The Effect of Excess Carrier on a Semiconducting Semi-Infinite Medium Subject to a Normal Force by Means of Green and Naghdi Approach

Ahmed E. Abouelregal [1,2] · Hamid M. Sedighi [3,4] · Ali H. Shirazi [3]

Received: 14 June 2021 / Accepted: 20 July 2021 / Published online: 28 July 2021

Abstract

For engineers and physicists, it is important to investigate the excitement of thermoelastic vibrations by photothermal effects since they are used in many fields. For this purpose, the photo-thermoelastic waves throughout the photothermal process for a semiconducting half-space have been investigated in this work. In contrast to many scientists who ignore the coupling effects between plasma and thermoelasticity, the influences of thermoelastic, carrier recombination and electronic elastic deformations on the semiconductor solids have been studied here. One of the thermoelastic theories which is appropriate for the limited speeds of heat waves has been considered. To solve the non-dimensional system resulting from generalized thermal elasticity theory without dissipating energy, coupled plasma, elastic wave and thermal wave equations, the normal mode technique has been applied. The amplitude expression for the field variables have been derived and graphically displayed. The numerical results have been verified and the influence of various factors has been also studied. In addition, several special cases of interest have been deduced. The analysis showed that the effective parameters have important effects on the physical fields by applying the presented model.

Keywords Photothermal · Thermoelasticity · Plasma-elastic wave · Half-space · Carrier recombination

1 Introduction

Thermoelasticity is a phenomenon in which the temperature changes through an elastic body leads to thermal stresses. The physical changes in size and shape of the elastic continuum arise due to the use of thermal energy or simply because the temperature changes are responsible for the above-mentioned changes in the material. The conventional uncoupled thermoelasticity theory (UCTE) predicts two incompatible physical phenomena. First, the mentioned theory does not involve elastic terms in the heat conduction equation. Secondly, the parabolic heat equation, predicts an unlimited rate of spread of the heat wave. Biot [1] developed the coupled theory of thermoelasticity (CTE) to remove the contradiction of UCTE theory which declared that elastic variations had no influence on temperature. For both diffusion theories, the heat equations forecast infinite propagation speeds for thermal waves toward physical observations.

At present, several theories of hyperbolic thermal elasticity have been advanced that allow finite speeds of heat waves. Among these theories that have been presented in this area, the theories of Lord and Shulman [2] and Green and Lindsay [3] have been proposed. These models treat the phenomenon of unlimited thermal wave propagation speed. Green and Naghdi [4] formulated another generalized theory called the thermoelasticity theory without dissipating energy. The gradients of thermal displacement

✉ Hamid M. Sedighi
h.msedighi@scu.ac.ir; ali.h.shirazimain@gmail.com

Ahmed E. Abouelregal
ahabogal@gmail.com

1 Department of Mathematics, College of Science and Arts, Jouf University, Al-Qurayyat, Saudi Arabia

2 Department of Mathematics, Faculty of Science, Mansoura University, Mansoura 35516, Egypt

3 Mechanical Engineering Department, Faculty of Engineering, Shahid Chamran University of Ahvaz, Ahvaz 61357-43337, Iran

4 Drilling Center of Excellence and Research Center, Shahid Chamran University of Ahvaz, Ahvaz, Iran

are included within their constitutive variables and differ from previous theories, as they do not allow heat dissipation. Tzou has proposed [5, 6] a model with dual-phase lag (DPL) that defines microscopic-level interactions among photons and electrons as sources that retard macroscopic responses. The macro-structural effect on the heat transfer behavior may be investigated using the DPL mode for macroscopic formulation. The experimental findings have supplemented the physical significance and applicability of DPL model [7]. Chandrasekharaiah [8] and Tzou [7] are proposing this dual-phase lag (DPL), which reflects a modified thermoelastic model in which the Fourier theory has been superseded by an approximation to a modified one with two separate delay times being, the heat flow phase delay and the thermal gradient phase delay.

In order to be able to recognize the physical realization of these materials, the interaction of light and nanoparticles between semiconductor materials is significant, because optical energy is absorbed and its employment in contemporary technology and physics. The photovoltaic energy results in the high vibrational behavior of particles so that the governing equation of the model with the concept of thermoelasticity is also explained. In photothermal theory, the influence of the thermal field on the elastic deformations of the semiconductor is typically studied. The overlap between photoexcited and thermal spaces is very significant for understanding the action of temperature distribution by the stress stream and semiconductor that has a broad range of applications in plasma physics.

The fundamental equations of the generalized theory of thermoelasticity are implemented to analyze semiconducting materials like an elastic body without taking into account light impact (neglecting electrons and thermoelasticity coupling). The interaction between thermal and elastic waves is explored in this case. In the process of the carrier recombine with the diffusion mechanism in a semiconductor medium, there are several theoretical and experimental studies to explain the superposition of thermal- elastic- plasma waves. The transmitting method for optical/acoustic frequencies explains the process of electronic distortions in one dimension in the sense of semiconductor optical theory [9].

Song et al. [10, 11] investigated thermoelastic vibrations due to microcantilevers of an optical semiconductor. Moreover, the reflection in a semiconductor material of plane waves into photothermal theories has also been studied [12, 13]. Hobiny and Abbas [14] analyzed a 2D problem for a semiconducting material using the energy dissipation (GN III) model proposed by Green and Naghdi. In a semiconductor medium with a spherical cavity and infinite one, Alzahrani and Abbas [15, 16] applied the Green and Naghdi model (Type III) under the two-temperature hyperbolic model. In an isotropic, homogeneous semiconducting medium Othman et al. [17] used Lord and Shulman model to investigate the time effect on photothermal waves. Abo-Dahab [18] addressed the influences of initial stress and magnetic field on photo-thermal wave reflection in the semiconductor media, taking classical and dual-phase-lag (DPL) models into consideration. In several external areas, several authors have studied different problems with generalized thermoelasticity with various boundary conditions with and without using the effect of photothermal excitation [19–28].

The expansion of spatially resolved study in situ to conceptualize transport processes in solids has gotten a lot of interest. While following a photothermal approach that can be seen as expansions of the photothermal aberrations methodology, we strive to ensure that the transfer process is established on the basis of photothermal beam aberrations. These methods are distinguished by the fact that they do not require any contact and immediately produce electronic and heat transport parameters on semiconducting surfaces, at the interface, and within most semiconducting materials. Pure silicon is a real semiconductor that is employed in a variety of applications in the semiconductor industry. Monocrystalline Si, for example, are utilized to make silicon wafers.

The spread of waves into thermoelastic materials is of great interest in various fields of science and technologies such as nuclear, automotive, thermal and submarine engineering, aerospace, chemical and pipeline technologies. Many researchers investigated the impact of thermoelastic and electronic deformation on the semiconductor media without considering the combination of plasma and thermoelastic effects. The contribution of this work is to present the photothermal and thermoelastic interactions within a solid half-space in the context of generalized Green and Naghdi theory. Plasma control equations and thermal behavior of the solid are given based on thermoelasticity and photothermal theories. The process of interference between elastic, thermal and plasma waves occurs by considering the transfer of thermal process. In addition, unlike many other contributions, the generalized thermoelasticity theories have been used instead of solving steady-state temperature equation. As a result, an extended hyperbolic thermoelastic model, which admits the propagation of thermal wave at a limited speed, is better suited to model these important issues.

In this work, during the photothermal process, the effect of the thermal and mechanical force in a half-space is studied. It is taken into account that the body is a two-dimensional semiconductor medium and that its boundaries are stress-free and thermally insulated. The governing equations of the problem are solved to provide solutions to surface waves, whether thermal, optical or mechanical. The distributions of the density of the thermal stress, carrier, temperature and displacements have been attained and analyzed. Some comparisons showed in figures to investigate the influence of the plasma and thermal waves on all the areas studied. In order to illustrate the physical sense of the problem, the effect of thermoelastic coupling and the lifetime of the photon-generated in the physical field have been graphed and analyzed.

2 Basic Equations

For thermoelastic semiconductors with isotropic and homogeneous electronic, thermal and elastic properties, the equations for coupled plasma, heat transport equation without energy dissipation and elastic equations are [4, 12, 29]:

Equations of motion:

$$(\lambda + \mu)\overrightarrow{\nabla}(\mathrm{div}(\boldsymbol{u})) + \mu\nabla^2\boldsymbol{u} - \gamma\nabla\theta - \delta\nabla N = \rho\frac{\partial^2\boldsymbol{u}}{\partial t^2}. \tag{1}$$

Where $\theta = T - T_0$ indicates the temperature change, $\boldsymbol{u}$ displacement vector, N is the carrier density, T_0 is the reference temperature, $\gamma = (3\lambda + 2\mu)\alpha_t$, α_t is the linear thermal expansion coefficient, ρ is density, $\delta = (3\lambda + 2\mu)d_n$ are the difference in the conductive and valence band deformation potential, λ, μ being Lamés constants.

The generalized hyperbolic heat equation without energy dissipation can be written as [4, 12]:

$$K^*\nabla^2\theta = \frac{\partial^2}{\partial t^2}[\rho C_E\theta + \gamma T_0(\mathrm{div}(\boldsymbol{u}))] - \frac{E_g}{\tau}\frac{\partial N}{\partial t} - \frac{\partial Q}{\partial t}. \tag{2}$$

Where C_E is the specific heat at constant strain, E_g is the semiconductor gap energy, Q is the heat supplied, τ is the lifetime of photogenerated electron-hole pairs, K^* is a material constant characteristic GN theory. In Eq. (2), the term $\frac{E_g}{\tau}\frac{\partial N}{\partial t}$ covers the effects of carrier volume heat generation and sample surface excitation.

The coupled plasma wave equation is given by the equation [12, 29].

$$D_E\nabla^2 N - \frac{1}{\tau}N - \rho\frac{\partial N}{\partial t} = \kappa\theta \tag{3}$$

Where D_E is the diffusion coefficient and κ is the thermal activation coupling parameter.

The components of the strain tensor:

$$e_{ij} = \frac{1}{2}\left(u_{i,j} + u_{j,i}\right). \tag{4}$$

The constitutive stress equations are given by:

$$\boldsymbol{\sigma} = \lambda(\mathrm{div}(\boldsymbol{u}))\boldsymbol{I} + \mu\left(\nabla\boldsymbol{u} + \nabla\boldsymbol{u}^{\mathrm{Tr}}\right) - (\gamma\theta + d_n N)\boldsymbol{I}. \tag{5}$$

Where $\boldsymbol{\sigma}$ is the stress tensor, Tr refers to the matrix transposition and $\boldsymbol{I}$ to the matrix identity.

3 The Problem Formulation

In this analysis, we examine a two-dimensional problem, including a homogeneous photo-thermoelastic, isotropic semiconductor solid, $(z \geq 0)$ with the z-axis indicating inside the half-space. This medium is subjected to a normal force on the plane surface $(z = 0)$ depending on the time t and the coordinate x, $(-\infty < x < \infty)$. In addition, we suppose that there is no body power or heat sources in the body and that the surface $(z = 0)$ is at rest initially and traction-free. Cartesian coordinate system (x, y, z) is used to analyze the problem. Since the nature of the proposed problem is two-dimensional, the present study will be restricted to the parallel planes of the x-z plane (Fig. 1). Thus all the studied functions will be dependent on x, z and t variables.

The displacement vector components and dilation can be written in the form

$$\boldsymbol{u} = (u, 0, w), \tag{6}$$

$$e = \mathrm{div}(\boldsymbol{u}) = \frac{\partial u}{\partial x} + \frac{\partial w}{\partial z}. \tag{7}$$

To present the basic equations more simply, we will define displacements u and w as functions in displacement potentials Φ and Ψ as follows

$$u = \frac{\partial\Phi}{\partial x} - \frac{\partial\Psi}{\partial z}, \quad w = \frac{\partial\Phi}{\partial z} + \frac{\partial\Psi}{\partial x}. \tag{8}$$

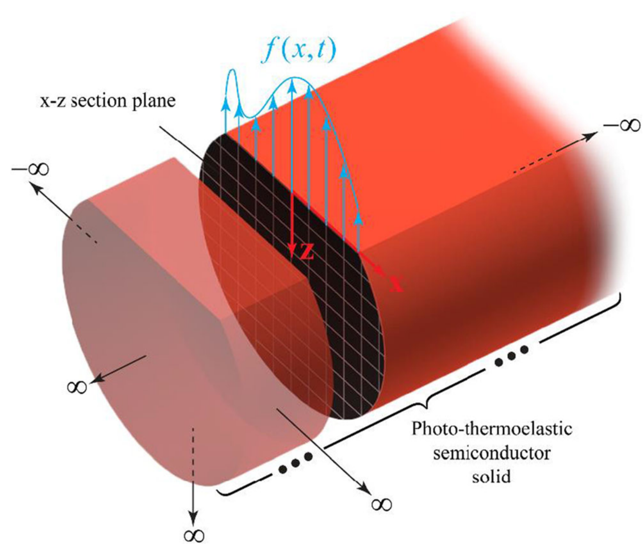

Fig. 1 Schematic of the proposed problem

Using potentials Φ and Ψ, then governing Eqs. (1)–(5) can be expressed as

$$c_1^2\nabla^2\Phi - \ddot{\Phi} = \frac{1}{\rho}(\gamma\theta + d_n N), \quad c_1^2 = \frac{\lambda + 2\mu}{\rho}, \tag{9}$$

$$c_2^2\nabla^2\Psi = \ddot{\Psi}, \quad c_2^2 = \frac{\mu}{\rho}, \tag{10}$$

$$K^*\nabla^2\theta = \frac{\partial^2}{\partial t^2}\left[\rho C_E\theta + \gamma T_0\nabla^2\Phi\right] - \frac{E_g}{\tau}\dot{N}, \tag{11}$$

$$D_E\nabla^2 N - \rho\dot{N} - \frac{1}{\tau}N = \kappa\theta, \tag{12}$$

$$\begin{aligned} \sigma_{xx} &= \lambda\nabla^2\Phi + 2\mu\frac{\partial}{\partial x}\left(\frac{\partial\Phi}{\partial x} - \frac{\partial\Psi}{\partial z}\right) - \gamma\theta - d_n N, \\ \sigma_{zz} &= \lambda\nabla^2\Phi + 2\mu\frac{\partial}{\partial z}\left(\frac{\partial\Psi}{\partial x} + \frac{\partial\Phi}{\partial z}\right) - \gamma\theta - d_n N, \\ \sigma_{xz} &= 2\mu\frac{\partial^2\Phi}{\partial x\partial z} + \mu\left(\frac{\partial^2\Psi}{\partial x^2} - \frac{\partial^2\Phi}{\partial z^2}\right). \end{aligned} \tag{13}$$

For simplicity, the non-dimensional variables illustrated below are considered suitable for implementation.

$$\begin{gathered} \left\{x', z', u', w'\right\} = \frac{\eta_0}{c_1}\{x, z, u, w\}, \quad t' = \eta_0 t, \quad \left\{\theta', N'\right\} = \frac{1}{\rho c_1^2}\{\gamma\theta, d_1 N\}, \\ \left\{\Phi', \Psi'\right\} = \frac{\eta_0^2}{c_1^2}\{\Phi, \Psi\}, \quad \sigma'_{ij} = \frac{\sigma_{ij}}{\mu}, \quad \eta_0 = \frac{\rho C_E c_1^2}{K^*}. \end{gathered} \tag{14}$$

The governing Eqs. (9)–(13), after the dimensionless parameters are presented, take the following form, in which the primes are dropped for convenience:

$$\nabla^2\Phi - \ddot{\Phi} = \theta + N, \tag{15}$$

$$\nabla^2\Psi = \beta^2\ddot{\Psi}, \tag{16}$$

$$\nabla^2\theta = \frac{\partial^2}{\partial t^2}\left[\eta_0\theta + \varepsilon_1\nabla^2\Phi\right] - \varepsilon_2\dot{N}, \tag{17}$$

$$\nabla^2 N = g_1\dot{N} + g_2 N + g_3\theta, \tag{18}$$

$$\begin{aligned} \sigma_{xx} &= \left(\beta^2 - 2\right)\nabla^2\Phi + 2\frac{\partial}{\partial x}\left(\frac{\partial\Phi}{\partial x} - \frac{\partial\Psi}{\partial z}\right) - \beta^2(\theta + N), \\ \sigma_{zz} &= \left(\beta^2 - 2\right)\nabla^2\Phi + 2\frac{\partial}{\partial z}\left(\frac{\partial\Psi}{\partial x} + \frac{\partial\Phi}{\partial z}\right) - \beta^2(\theta + N), \\ \sigma_{xz} &= 2\frac{\partial^2\Phi}{\partial x\partial z} + \frac{\partial^2\Psi}{\partial x^2} - \frac{\partial^2\Phi}{\partial z^2}, \end{aligned} \tag{19}$$

where

$$\begin{gathered} \beta^2 = \frac{\lambda + 2\mu}{\mu}, \quad \varepsilon_1 = \frac{\gamma^2 T_0}{\rho K^*}, \quad \varepsilon_2 = \frac{\gamma E_g c_1^2}{\tau d_n K^*}, \\ g_1 = \frac{\rho c_1^2}{D_E\eta_0}, \quad g_2 = \frac{c_1^2}{D_E\eta_0\tau}, \quad g_3 = \frac{\kappa d_n c_1^2}{D_E\eta_0^2}. \end{gathered} \tag{20}$$

4 Solution of the Problem

Different methods and algorithms were introduced to approximate the behavior/solution of ordinary/partial differential eqs. (O/PDEs) using specific functions which are explicitly designed to show certain desirable features [30–40]. Deep Neural Networks (DNNs) have been utilized as an alternative like those proposed by Samaniego et al. [41]. They achieved remarkable success in different areas such as visual recognition. In the subject of computational analysis to deal with different partial differential equations, Rabczuk et al. [42] developed a novel nonlocal operator theory based on the variational principle. In their research, common differential operators and variational forms were defined by employing nonlocal operators. Using artificial neural networks and an adaptive collocation technique, Anitescu et al. [43] demonstrated a novel technique for solving partial differential equations. Initially, a crude grid of training points was utilized, but when the residual value at a wider set of assessment sites increases, additional points were then added.

Without any supposed constraints on field variables, the normal mode analysis provides accurate solutions. The normal mode analysis actually includes the search for the solution in the Fourier domain, provided that all field quantities on the real line are smooth enough for the normal mode analysis to be carried forward. Cheng and Zhang [44] proposed a standard method for modeling an elastic heat treatment of an elastic waveform on an isotropic plate.

for normal modes, the solution to the domain variables under analysis can be imposed as follows

$$\begin{aligned} &\left\{u, w, \theta, \Phi, \Psi, N, \sigma_{ij}\right\}(x, z, t) \\ &= \left\{u^*, w^*, \theta^*, \Phi^*, \Psi^*, N^*, \sigma_{ij}^*\right\}(x)\mathrm{e}^{\omega t + iaz}, \end{aligned} \tag{21}$$

Where $i = \sqrt{-1}$, ω is the frequency and a denotes the z-direction wave number. Using Eq. (21), Eqs. (15)–(19) can be introduced as

$$\left(\frac{\mathrm{d}^2}{\mathrm{d}x^2} - \zeta_1\right)\Phi^* = \theta^* + N^*, \tag{22}$$

$$\varepsilon_1\omega^2\left(\frac{\mathrm{d}^2}{\mathrm{d}x^2} - a^2\right)\Phi^* = \left(\frac{\mathrm{d}^2}{\mathrm{d}x^2} - \zeta_2\right)\theta^* + \varepsilon_2\omega N^*, \tag{23}$$

$$\left(\frac{\mathrm{d}^2}{\mathrm{d}x^2} - \zeta_3\right)N^* = g_3\theta^*, \tag{24}$$

$$\left(\frac{\mathrm{d}^2}{\mathrm{d}x^2} - \xi^2\right)\Psi^* = 0, \tag{25}$$

$$\sigma^*_{xx} = \left[\beta^2 \frac{d^2}{dx^2} - a^2\left(\beta^2 - 2\right)\right]\Phi^* - 2ia\frac{d\Psi^*}{dx} - \beta^2\left(\theta^* + N^*\right),$$
$$\sigma^*_{zz} = \left[\left(\beta^2 - 2\right)\frac{d^2}{dx^2} - \beta^2 a^2\right]\Phi^* + 2ia\frac{d\Psi^*}{dx} - \beta^2\left(\theta^* + N^*\right),$$
$$\sigma^*_{xz} = a\left(2i\frac{d}{dx} + a\right)\Phi^* + \frac{d^2\Psi^*}{dx^2}, \tag{26}$$

where $\zeta_1 = a^2 + \omega^2$, $\zeta_2 = a^2 + \eta_0\omega^2$, $\zeta_3 = a^2 + g_1\omega + g_2$.and $\xi^2 = a^2 + \omega^2\beta^2$. Removing $\theta^*(x)$ and $N^*(x)$ in Eqs. (22)–(24), we have

$$\left(\frac{d^6}{dx^6} - A\frac{d^4}{dx^4} + B\frac{d^2}{dx^2} - C\right)\Phi^* = 0, \tag{27}$$

with

$$A = \zeta_1 + g_7 + \frac{g_6}{g_3}, \quad B = \zeta_1 g_7 + g_8 + a^2 + g_5, \quad C = \frac{a^2 g_5 g_6}{g_3},$$
$$g_5 = \zeta_1 - g_3, \quad g_6 = \varepsilon_1\omega^2 g_3, \quad g_7 = \zeta_2 + \zeta_3, \quad g_8 = \zeta_2\zeta_3 + \varepsilon_2\omega g_3. \tag{28}$$

Factorizing the differential eq. (27), yields to:

$$\left(\frac{d^2}{dx^2} - k_1^2\right)\left(\frac{d^2}{dx^2} - k_2^2\right)\left(\frac{d^2}{dx^2} - k_3^2\right)\Phi^* = 0, \tag{29}$$

where k_n^2, $n = 1,2,3$ are the roots of the equation

$$k^6 - Ak^4 + Bk^2 - C = 0. \tag{30}$$

The general solution of Eq. (29) which is bounded at $x \to \infty$, can be expressed as

$$\Phi^*(x) = \sum_{n=1}^{3} C_n e^{-k_n x}. \tag{31}$$

In a similar way, we obtain

$$\left\{N^*, \theta^*\right\}(x) = \sum_{n=1}^{3}\left\{C'_n, C''_n\right\}e^{-k_n x}, \tag{32}$$

Inserting Eqs. (31) and (32) into Eqs. (22) and (24), we obtain the following relation:

$$C'_n = H_n C_n, \quad C''_n = L_n C_n, \tag{33}$$

where

$$H_n = \frac{g_3\left(k_n^2 - \zeta_1\right)}{k_n^2 - g_5}, \quad L_n = \frac{\left(k_n^2 - \zeta_1\right)\left(k_n^2 - \zeta_3\right)}{k_n^2 - g_5}. \tag{34}$$

The general solution of Eq. (25) is given by

$$\Psi^*(x) = C_4 e^{-\xi x}. \tag{35}$$

Making use of solutions given in Eqs. (31) and (35), one gets

$$u^*(x) = -\sum_{n=1}^{3} k_n C_n e^{-k_n x} - iaC_4 e^{-\xi x},$$
$$w^*(x) = ia\sum_{n=1}^{3} C_n e^{-k_n x} - \xi C_4 e^{-\xi x}. \tag{36}$$

Substituting Eqs. (31), (32) and (35) into Eqs. (26), we obtain

$$\sigma^*_{xx} = \sum_{n=1}^{3} P_n C_n e^{-k_n x} + 2ia\xi C_4 e^{-\xi x},$$
$$\sigma^*_{zz}(x) = \sum_{n=1}^{3} R_n C_n e^{-k_n x} - 2ia\xi C_4 e^{-\xi x}, \tag{37}$$
$$\sigma^*_{xz}(x) = \sum_{n=1}^{3} Q_n C_n e^{-k_n x} + \xi^2 C_4 e^{-\xi x},$$

where

$$R_n = k_n^2\left(\beta^2 - 2\right) - \beta^2\left(H_n + L_n + a^2\right), \quad Q_n = -2iak_n + a^2,$$
$$P_n = \beta^2 k_n^2 - \beta^2\left(H_n + L_n + a^2\right) + 2a^2. \tag{38}$$

5 Parameter Study

In this section, the parameters C_j, $j = 1,2,3,4$ are determined. We can suppress the positive exponentials in the physical problem, which are unbounded at infinity. We assume that on the bounding plane ($x = 0$) of the medium thermally insulated and subjected to a normal force that depends on t and x variables. The non-dimensional mechanical and thermal boundary conditions of the problem on the boundary surface $z = 0$ may be taken as

$$\sigma_{zz}(0, z, t) = -P = -P_0 e^{\omega t + iaz}, \quad \sigma_{xz}(0, z, t) = 0. \tag{39}$$

$$\left.\frac{\partial\theta}{\partial x}\right|_{x=0} + h\theta(0, z, t) = 0. \tag{40}$$

The carriers will enter the sample surface during the diffusion process, with a limited potential for recombination. So the boundary condition for carrier density may be expressed as

$$D_E\left.\frac{\partial N}{\partial x}\right|_{x=0} = s_f N(0, z, t), \tag{41}$$

Where the constant s_f is the speed of recombination of the surface.

The following equations are readily satisfied by the parameters C_j, $j = 1, 2, 3, 4$ by substituting the expressions of the field variables σ_{zz}, σ_{xz}, θ and N into Eqs. (39)–(41):

$$\sum_{n=1}^{3} R_n C_n - 2ia\xi C_4 = -P_0, \tag{42}$$

$$\sum_{n=1}^{3} Q_n C_n + \xi^2 C_4 = 0, \tag{43}$$

$$\sum_{n=1}^{3} G_n C_n e^{-k_n x} = 0, \tag{44}$$

$$\sum_{n=1}^{3} U_n C_n = 0, \tag{45}$$

where

$$G_n = H_n(D_E k_n + s_f), \qquad U_n = L_n(h - k_n). \tag{46}$$

In the form of a system of matrices, the solutions of the equations can be expressed as

$$\begin{Bmatrix} C_1 \\ C_2 \\ C_3 \\ C_4 \end{Bmatrix} = \begin{bmatrix} R_1 & R_2 & R_3 & -2ia\xi \\ Q_1 & Q_2 & Q_3 & \xi^2 \\ G_1 & G_2 & G_3 & 0 \\ U_1 & U_2 & U_3 & 0 \end{bmatrix}^{-1} \begin{Bmatrix} -P_0 \\ 0 \\ 0 \\ 0 \end{Bmatrix}. \tag{47}$$

We have the values of the four constants C_j, $j = 1, 2, 3, 4$ after applying the inverse of the matrix technique.

6 Numerical Results

Numerical methods are used to anticipate the reaction or behavior of a system in a variety of applications including mechanical systems, structural reliability, material modelling, and etc. [45]. Calibrating and validating the mathematical models as well as determining how much the model output is affected by changes in input parameters, is critical. For these objectives, sensitivity analysis (SA) comes in handy [46]. As a result, researchers in several disciplines, such as material modelling and structural design, have lately been interested in uncertainty and sensitivity analysis. For this purpose, estimating the impact of altering several parameters on the model outputs at the same time is more realistic. In order to build a SA, it is critical to understand the relationships between the unknown input parameters [47]. However, since our main objective is to show the excitement of thermoelastic vibrations by photothermal effects, the SA is neglected here for the sake of clarity.

We are now presenting some computational numerical results to explain the theoretical findings of the previous section. For a small-time value of $t = 0.02$ s, the calculations are performed. The value for the related parameters for the isotropic thermoelastic solid at $T_0 = 298$ K is taken as [15, 16].

$$K = 2.510 \text{ W m}^{-1}\text{K}^{-1}, \quad \rho = 1740 \text{ kg m}^{-3},$$

$$d_n = -9 \times 10^{-31} \text{ m}^3, E_g = 1.11 \text{ eV}, \quad \mu = 1.639 \times 10^{10} \text{kg m}^{-1}\text{s}^{-2},$$

$$\lambda = 2.696 \times 10^{10} \text{kg m}^{-1}\text{s}^{-2}, C_E = 1.04 \times 10^3 \text{ J kg K}^{-1},$$

$$s_f = 2 \text{ m s}^{-1}, \quad D_E = 2.5 \times 10^{-3} \text{ m}^2 \text{ s}^{-1}, \quad \tau = 5 \times 10^{-5} \text{ s}.$$

Since we have the angular frequency ω in a complex form, it can therefore be written on the form $\omega = \omega_0 + i\xi$, $e^{\omega t} = e^{\omega_0 t}[\cos(\xi t) + i\sin(\xi t)]$. We may take angular frequency as a real number for small values of time, and thus, we can choose $\omega = \omega_0 = 2$. Also, for the non-dimensional quantity $\eta_0 = \rho C_E c_1^2 / K^*$, we will consider the default value $\eta_0 = 2$.

In this analysis, we will use the above-mentioned parameters to measure the numerical values of the real part for all different fields. The behavior of the distributions of the components of the normal displacement u, tangential displacement w, normal force stress σ_{zz}, tangential stress σ_{zx}, temperature distribution θ, carrier charge density N versus the distance change x at the $z = 1$ plane will be studied. Also during this numerical discussion, we will study the effect of some factors affecting the response of different fields. Comparisons and studies were made between these dimensional physical quantities through three different cases.

The variations in the fields examined are shown in Figs. 2-19. By observing the given figures, it was found that the heat wave front moves in the medium with a finite speed over time. This phenomenon does not occur in the classical theories of thermal elasticity, which is inherent in infinite propagation velocity, and that all physical quantities studied at each point in the medium have a non-zero value. These results indicate that the presented model of hyperbolic photo-thermoelasticity is more suitable than the Fourier model of thermal conductivity.

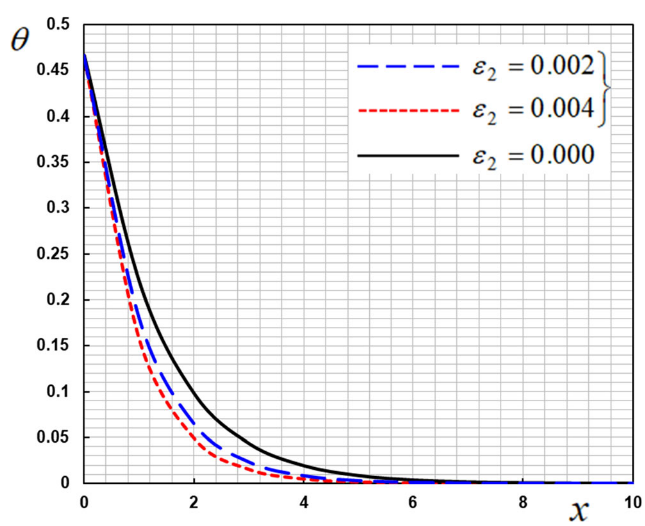

Fig. 2 The temperature θ versus x under the effect of the parameter ε_2

6.1 Influence of the Thermoelastic Coupling Parameter

The term $\gamma T_0 \frac{\partial^2}{\partial t^2}(\mathrm{div}(\boldsymbol{u}))$ in the heat eq. (2) represents the heat–strain coupling, and this term is neglected in the unconventional thermoelasticity theory. In the unconventional theory, the effect of excitation on heat waves is ignored which conflicts with physical experiences in the real world. In this section, the influence of existence and absence of thermoelastic coupling parameter ε_2 on different physical distributions will be discussed. Their consideration has been found to be important in many applications, such as vibration modeling of resonant micro-electromechanical systems (MEMS), dynamic crack propagation, thermal shocks, ultrafast laser heating in material heat treatment and wave propagation [48–50].

The results obtained for the studied fields against positions x in the range $0 \le x \le 10$ are compared and plotted in Figs. 2 to 7. It is clear from these figures that as x tends to infinity, all curves coincide and the field variables satisfy the assumed boundary conditions.

Figure 2 displays the temperature change θ across the distance x for three cases by taking the values $\varepsilon_2 = 0$, $\varepsilon_2 = 0.002$ and $\varepsilon_2 = 0.004$, which investigates the effect of thermoelastic coupling.

It is noticed that the temperature field begins with positive values of 4.666 for the two theories; the Green and Naghdi model (GN-II) and uncoupled theory (UCTE) respectively. The Figure demonstrates that there is a significant influence of the thermoelastic coupling parameter on the profile of temperature θ. For the three cases, this constant has qualitatively similar behavior. From the plot, it can also be shown that the parameter ε_2 acts to reduce the temperature field magnitude.

The variance of normal displacement variable u versus distance for various values of the thermoelastic coupling parameter is shown in Fig. 3. It can be seen from Fig. 3 that the vertical displacement starts with its largest value at the boundary surface $x = 0$ and then slowly reduces with increasing distance from this surface until it disappears completely. Increasing the parameter of the thermoelastic coupling results in an increase in the values of the displacement u. Therefore, it has a growing influence, but the qualitative behavior for all three values is almost the same.

Figure 4 shows the distribution of the vertical displacement w with the distance x. For all values of the parameter ε_2, the behavior of w is nearly the same. It is also found that due to the presence of coupling parameter, the displacement w has appreciably significantly for $\varepsilon_2 = 0.002$ and $\varepsilon_2 = 0.004$ compared to $\varepsilon_2 = 0$. An increase in the value of the coupling parameter ε_2 raises the values of the displacement w.

The differences in normal pressure σ_{zz} at distance x are shown in Fig. 5 for the values of the different coupling parameters. In all three situations, the field of thermal stress rises dramatically in the initial range and then decreases with the passing of time to zero. All curves in this figure have a starting point associated with the value $\sigma_{zz} = -1$, which indicates that the boundary conditions are met. The figure also indicates that the distribution of the stress σ_{zz} achieved for the GN-II model ($\varepsilon_2 = 0.002$, $\varepsilon_2 = 0.004$) has significant values than those obtained for the UCTE ($\varepsilon_2 = 0$), which indicates a lower influence of the coupled parameter on the thermal stress σ_{zz}.

The thermal stress variation σ_{zx} across the x-direction is shown in Fig. 6. The coupling parameter ε_2 is shown to raise the magnitude of the tangential stress σ_{zx}. The curves of the thermal stress variable σ_{zx} begin with zero values and satisfy the assumed boundary conditions.

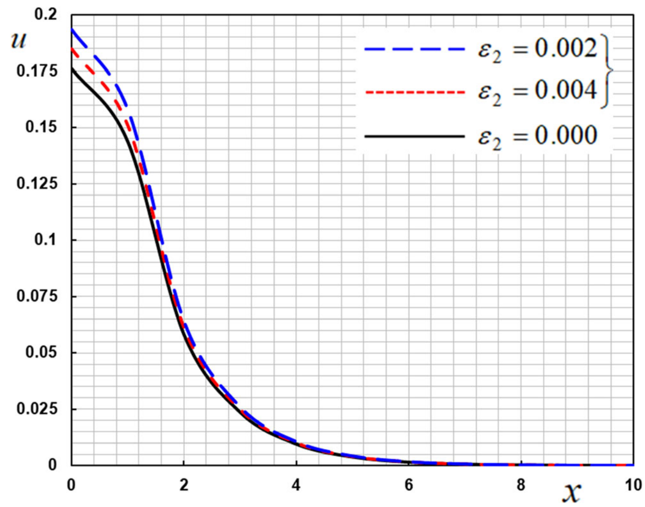

Fig. 3 The normal displacement u versus x under the effect of the parameter ε_2

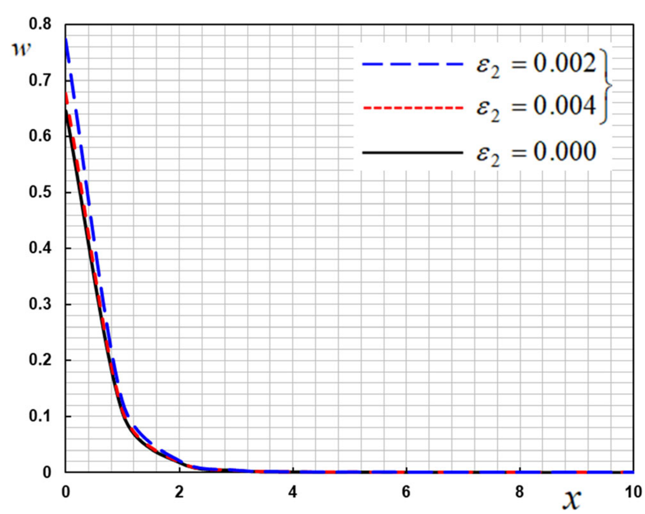

Fig. 4 The tangential displacement w versus x under the effect of the parameter ε_2

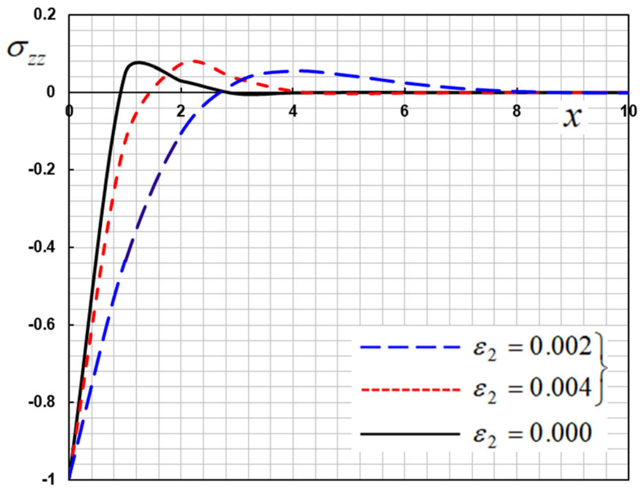

Fig. 5 The normal force stress σ_{zz} versus x under the effect of the parameter ε_2

Figure 7 shows the distributions of the carrier density N due to the effect of the thermo-coupling parameter ε_2 along the x-direction. Fig. 7 shows an important impact on the distributions of the carrier density N by the thermoelectric coupling parameter ε_2. Also, all distributions except for a thermal stress σ_{zx} have non-zero values only in a small half-space area. The values disappear outside of this area, which corresponds to the experimental results. This shows that the hyperbolic heat driving model concept is more physically practical than the Fourier thermal driving model.

The values also disappear beyond this area, which corresponds to experimental findings. It shows that a model based on the hyperbolic model is more realistic than a Fourier model. By comparing the solutions, it is inferred that in the case of the photothermoelastic model without energy dissipation (Type II), the coupled photothermoelastic models are significant phenomena and have major impacts on the distribution of field responses.

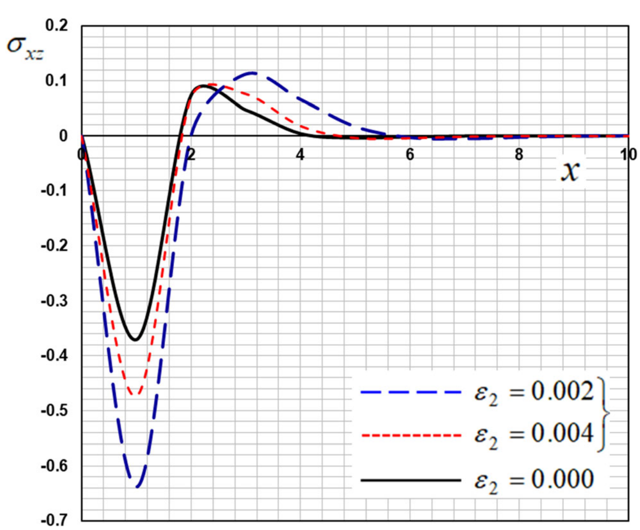

Fig. 6 The tangential force stress σ_{xz} versus x under the effect of the parameter ε_2

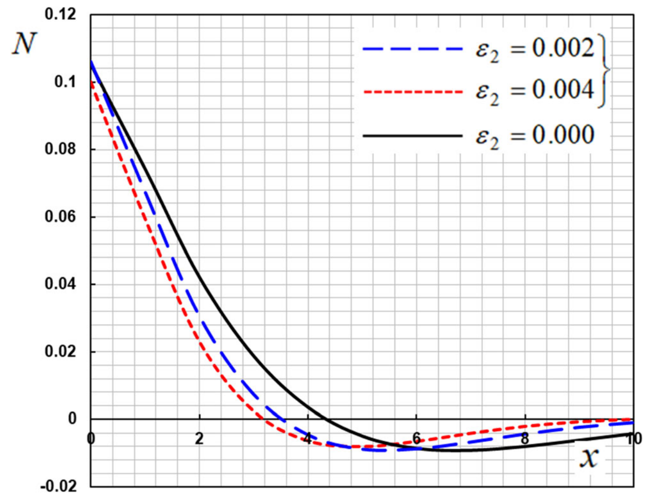

Fig. 7 The carrier charge density N versus x under the effect of the parameter ε_2

6.2 Influence of the Photo-Generated Carrier Lifetime Parameter

Electrons can be excited to higher energy states by semiconductors (for example, due to photon absorption), forming electron-hole pairs, and the process called generation. These electrons will fall back to their ground states through recombination at some later stage. Usually, the charge-carrier lifetime is defined as the average time it takes after excitation for electrons and holes to recombine. Since the lifetime of the charge-carrier is defined as this statistical average-which involves large populations of electrons and holes all recombining through multiple pathways at different times it cannot be precisely measured; in other words, it remains prohibitively difficult to track individual charge-carriers, summarize their individual lifetimes and calculate their average accurately.

As such, lifetime must somehow be inferred from another property in which both generation and recombination occur, such as photoluminescence, photoconductance, or photovoltaic response. One of the most significant primary parameters in a solar cell is the charge carrier lifetime. The diffusion length and, therefore, the likelihood of a photogenerated charge carrier reaching the respective electrode is described in combination with the mobility of the charge carrier.

According to the earlier explanations, the minority carrier lifetime is an essential physical characteristic which is directly connected to semiconductor recombination processes. A good-quality semiconductor with few defects has a long minority carrier lifetime, whereas a bad-quality semiconductor has a short minority carrier lifetime and high defect density. The minority carrier lifetime of a semiconductor, for example, have a significant impact on the switching speed of a bipolar junction transistor and the conversion efficiency of a p-n junction solar cell.

The variations of the studied fields due to the influence of the photo-generated carrier lifetime parameter τ against x are displayed in Figs. 8-13. We can see that the parameter τ has major influences on all the studied variables. In Fig. 8, the temperature distribution θ along the x-direction is presented for different values of the parameter τ. The temperature change θ increases with increasing the parameter τ. In Figs. 9 and 10, normal and vertical displacement distributions u and u are presented with respect to the parameter τ. It is noticed that with the rise of the parameter τ, the displacements decrease.

The effect of different carrier lifetime parameters τ on thermal stress σ_{zz} is shown in Fig. 11, where it is noted that the influence of τ for heat flux dominates here. In Fig. 12, versus x, the tangential stress σ_{zx} shows oscillatory behavior. The graph that shows the impact of the carrier lifetime parameter τ is dominant here. The tangential stress σ_{zx} values begin to decrease to a minimum value in the range $0 \leq x \leq 1$, then increase in the range $1 \leq x \leq 3$, and gradually decrease and go to zero in the range $3 \leq x \leq 6$. In Fig. 13, the distribution of N with respect to the parameter τ is displayed with respect to distance. The distribution of N increases with the increase of the parameter τ.

6.3 The Influence of Time Instant

Figures 14-19 display 3D curves to investigate the distributions of the physical fields with the distance x and instant time t changes. We can see that the instant time t affects all of the fields studied. In these figures, it is also observed that the values of the field variables in each fixed point (x, z) increase as the time t increases. Figs. 18 and 19 display that thermal

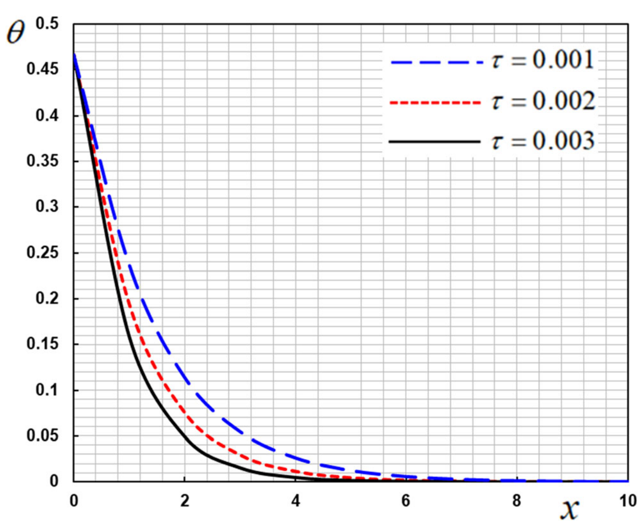

Fig. 8 The temperature θ under the effect of the parameter τ

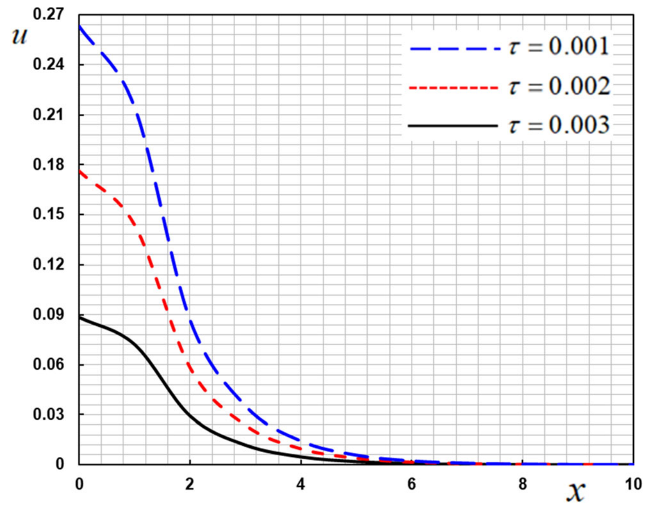

Fig. 9 The normal displacement u under the effect of the parameter τ

stress σ_{zz} and σ_{xz} fulfill the limiting condition at $x = 0$ having different behavior.

It is found that all studied distributions have non-zero values only in a limited spatial region. All values outside this region disappear in early times of the reactions which means that the region has not yet experienced thermal disturbances.

By comparing the illustrative results of these figures, it is concluded that in the distribution of different fields, the time parameter plays a significant role, because the amplitude of such quantities varies as the time increases. Finally, it becomes clear that the physical quantities depend on the x and z spaces in addition to time t.

7 Concluding Remarks

A new major branch of research is the theory of generalized optical thermoelastic theory with photothermal excitation. There are only a few studies focusing on this concept in the

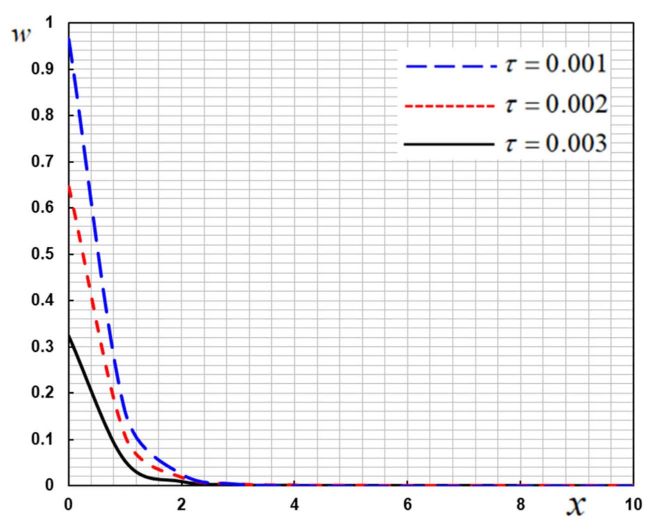

Fig. 10 The tangential displacement w under the effect of the parameter τ

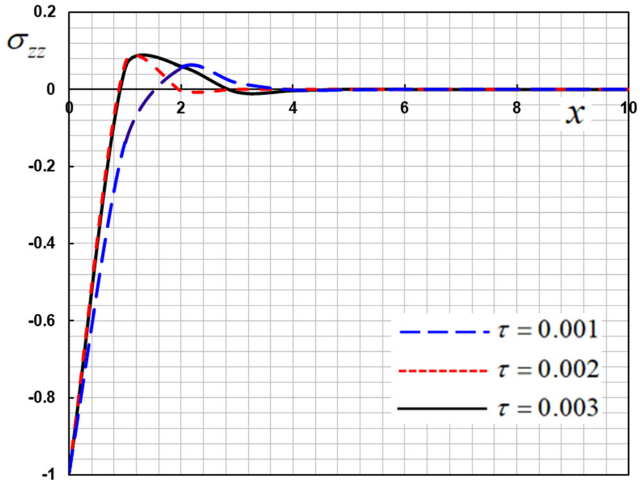

Fig. 11 The normal force stress σ_{zz} under the effect of the parameter τ

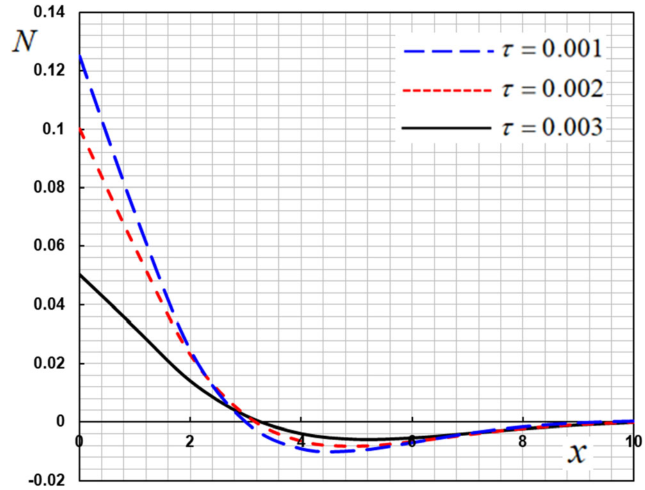

Fig. 13 The carrier charge density N under the effect of the parameter τ

literature. In the current research, we analysis the coupling of thermal waves, plasma and elastic waves in a thermoelastic semiconductor medium under the generalized model of type II proposed by Green-Naghdi. Based on the findings of this review, the following conclusions can be drawn:

- It is evident from all estimates that all field variables have non-zero values in a confined area. The values vanish symmetrically outside the region, which demonstrates that there has been no thermal turbulence in the region.
- Presence of coupling term in the heat equation have influenced all the studied fields. It decreases the temperature and carrier charge density while increasing the amount of displacements and the magnitude of thermal stresses.
- We observed a finite diffusion of the heat propagation in the medium from the temperature distributions. The heatwave forehead goes along with a finite speed of the medium, demonstrating that the Green and Naghdi model (GN-II) is very close to the physical performance of elastic materials.
- It is proved that the values all field variables are highly dependent on the carrier life parameter. There is also a significant difference in values for different time values in the studied fields.
- The method used in this work refers to a broad variety of thermodynamic and photo-thermal problems. This investigation can analyze and design the materials covered by thermal, plasma and a beat laser, as well as many engineering performances relevant to boundary examination and design.

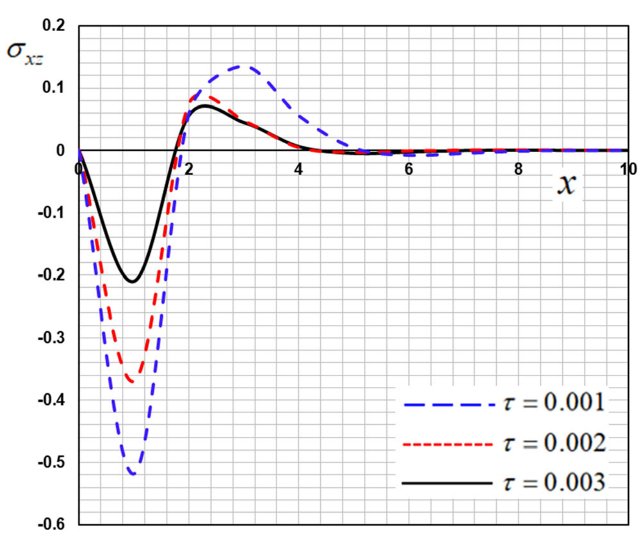

Fig. 12 The tangential force stress σ_{xz} under the effect of the parameter τ

8 Potential Applications

The stated results and analysis have significant importance in a variety of scientific branches. The extracted results are beneficial for any thermoelastic system that can be idealized as a semi-

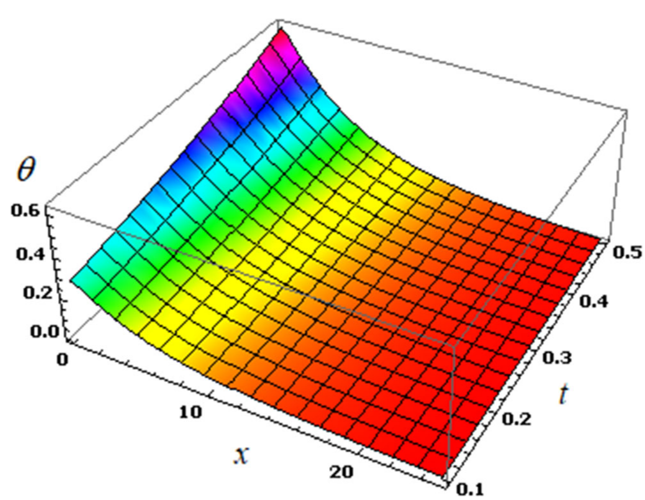

Fig. 14 The temperature θ versus distance x and instant time t

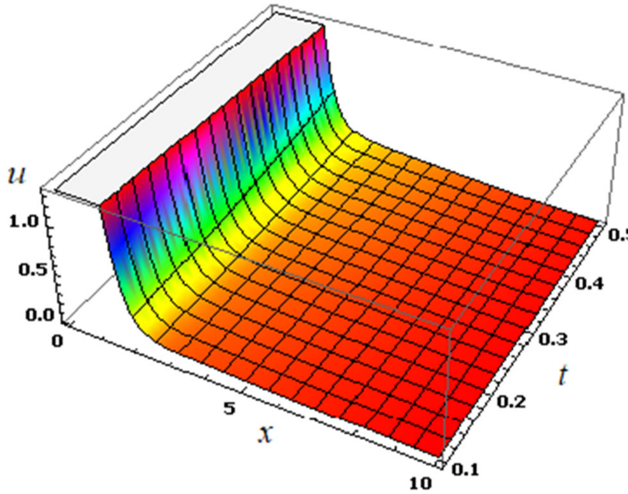

Fig. 15 The normal displacement u versus distance x and instant time t

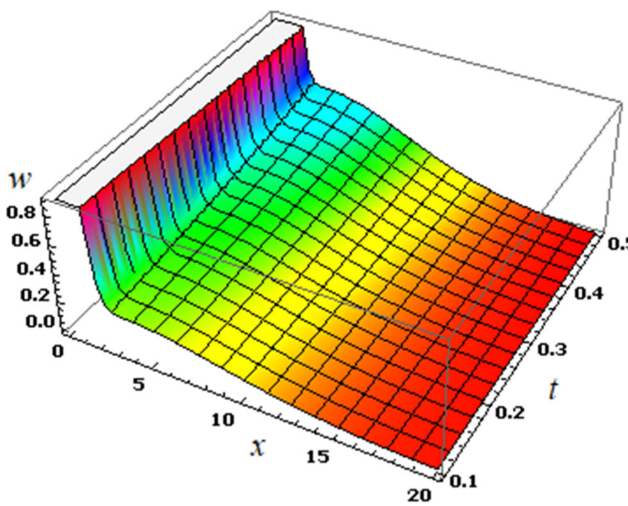

Fig. 16 The tangential displacement w versus distance x and instant time t

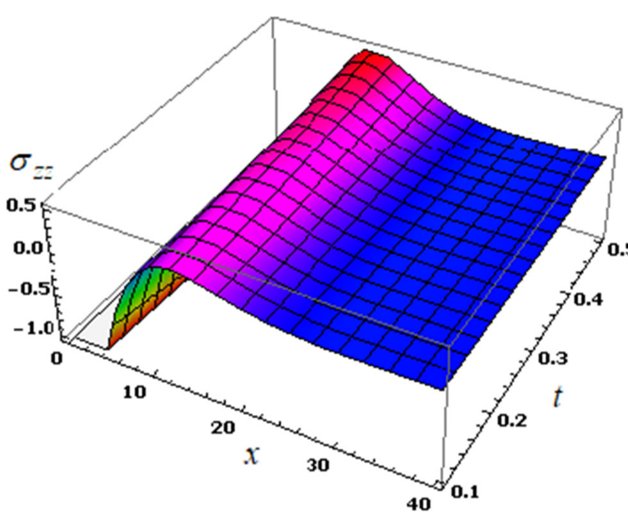

Fig. 17 The normal force stress σ_{zz} versus distance x and instant time t

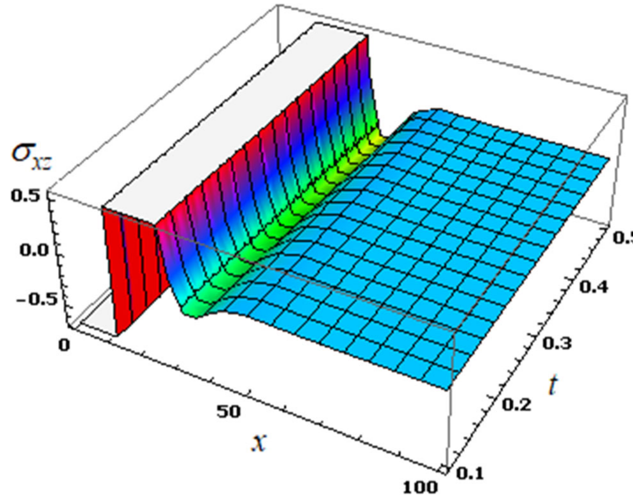

Fig. 18 The tangential force stress σ_{xz} versus distance x and instant time t

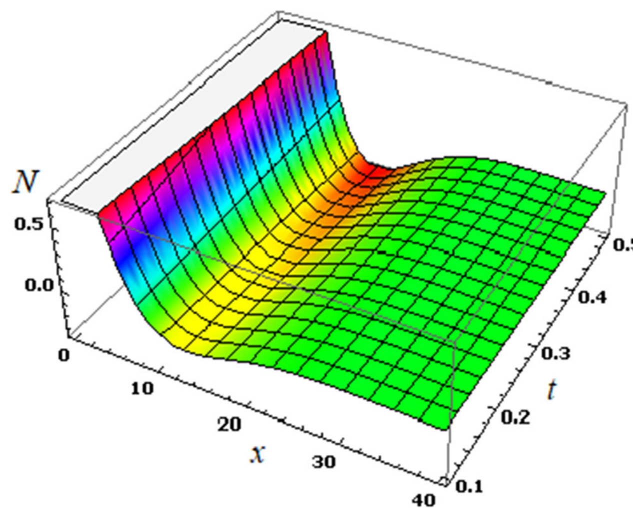

Fig. 19 The carrier charge density N versus distance x and instant time t

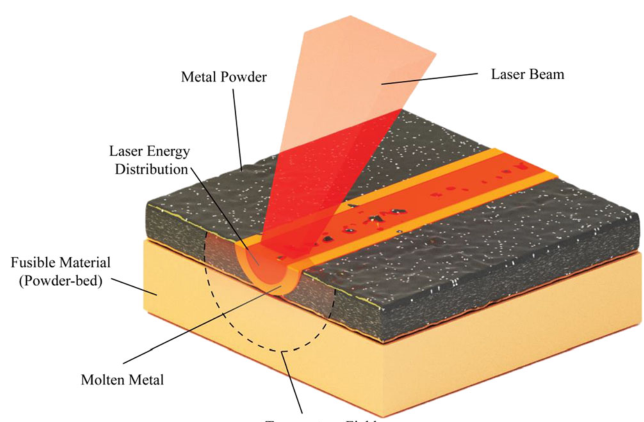

Fig. 20 Selective Laser Melting (SLM) and half-space fusible material

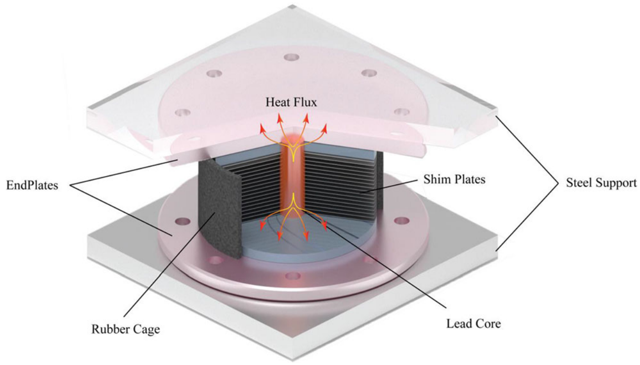

Fig. 21 Lead-Rubber Bearings and half space endplates

infinite medium. In principle, a semi-infinite solid (half-space) continues to infinity in all directions except one. As a result, the single surface characterizes the entire material. Most bodies can be assumed as a semi-infinite system if the interest of the analysis is limited to the immediate vicinity of the surface or the system's studied response is restricted to short periods. For instance, in the Selective Laser Melting (SLM) system, field variables (e.g. temperature field) can be studied by assuming the Powder-bed (fig. 20) as a half-space medium.

Another example of using the proposed procedure is in the heat generation of Lead-robber bearings. These kinds of bearings are used to isolate seismic waves and are mostly implemented in structural foundations to prevent earthquake damages. The lead core dissipates energy by resisting motion; as a result of core resistance, a significant amount of heat flows from the core to top and bottom endplates (fig. 21). The heat conduction through the circular endplates can be treated as a half-space problem as these endplates are mostly attached to structural girders and steel support. Therefore various field variables, for instance, the temperature which affects the performance of bearing, can be studied using the procedure explained in this study.

Dara Availability All data will be available upon the request of readers and/or the reviewers.

Code Availability All code data will be available upon the request of readers and/or the reviewers.

Authors' Contributions Author 1 planned the scheme and initiated the project and wrote the manuscript; Author 2 and Author 3 developed the mathematical modeling and examined the theory validation. The manuscript was written through the contribution of all authors. All authors discussed the results, reviewed, and approved the final version of the manuscript.

Funding H. M. Sedighi is grateful to the Research Council of Shahid Chamran University of Ahvaz for its financial support (Grant No. SCU.EM99.98).

Declarations

Ethics Approval The standard ethics of the journal are approved by all authors.

Consent to Participate Not Applicable.

Consent for Publication Not Applicable.

Conflicts of Interest/Competing Interests The authors declared no potential conflicts of interest with respect to the research, authorship, and publication of this article.

References

1. Biot M (1956) Thermoelasticity and irreversible thermodynamics. J Appl Phys 27:240–253
2. Lord H, Shulman Y (1967) A generalized dynamical theory of thermoelasticity. J Mech Phys Solid 15:299–309
3. A. E. Green and K.A. Lindsay, Thermoelasticity, J. Elast, 2, 1–7,
4. Green AE, Naghdi PM (1993) Thermoelasticity without energy dissipation. J Elast 31:189–209
5. Tzou DY (1996) Macro-to-microscale heat transfer: the lagging behavior. DC, Taylor & Francis, Washington
6. Tzou DY (1995) A unified approach for heat conduction fromMacro-toMicro-scales. J Heat Transf 117:8–16
7. Tzou DY (1995) Experimental support for the lagging behavior in heat propagation. J Thermophys Heat Transf 9:686–693
8. Chandrasekharaiah DS (1986) Thermoelasticity with second sound: a review, applied mechanics. Appl Mech Rev Mar vol 39(3):355–376
9. Todorović DM, Nikolić PM, Bojičić AI (1999) Photoacoustic frequency transmission technique: electronic deformation mechanismin semiconductors. J Appl Phys 85:7716–7726
10. Song Y, Todorović DM, Cretin B, Vairac P (2010) Study on the generalized thermoelastic vibration of theoptically excited semiconducting microcantilevers. Int J Solids Struct 47:1871–1875
11. Song Y, Todorovic DM, Cretin B, Vairac P, Xu J, Bai J (2014) Bending of semiconducting cantilevers under photothermal excitation. Int J Thermophys 35(2):305–319
12. Song Y, Bai J, Ren Z (2012) Reflection of plane waves in a semiconducting medium under Photothermal theory. Int J Thermophys 33:1270–1287
13. Song Y, Bai J, Ren Z (2012) Study on the reflection of photothermal waves in a semiconducting medium under generalized thermoelastic theory. Acta Mech 223:1545–1557
14. Hobiny A, Abbas I (2019) A GN model on photothermal interactions in a two-dimensions semiconductor half space. Results Phys 15:102588
15. Alzahrani FS, Abbas IA (2020) Photo-thermal interactions in a semiconducting media with a spherical cavity under hyperbolic two-temperature model. Mathematics 8:585
16. Alzahrani F, Abbas I (2020) The effect of a hyperbolic two-temperature model with and without energy dissipation in a semiconductor material. Mathematics 8:1711
17. Othman MIA, Tantawi RS, Eraki EEM (2016) Propagation of the photothermal waves in a semiconducting medium under L-S theory. J Therm Stresses 39(11):1419–1427
18. Abo-Dahab SM (2020) P-waves reflection in a semiconducting photothermal diffusion medium with initial stress and magnetic field. Mechanics Based Design of Structures and Machines:1–21. https://doi.org/10.1080/15397734.2020.1801462
19. Abouelregal AE (2020) Magneto-photothermal interaction in a rotating solid cylinder of semiconductor silicone material with time dependent heat flow. Appl Math Mech-Engl Ed 42:39–52. https://doi.org/10.1007/s10483-021-2682-6

20. Abouelregal AE (2020) Modified fractional photo-Thermoelastic model for a rotating semiconductor half-space subjected to a magnetic field. Silicon 12:2837–2850
21. Abouelregal, A. E., Modified fractional thermoelasticity model with multi-relaxation times of higher order: Application to spherical cavity exposed to a harmonic varying heat. Waves in Random and Complex Media, 1–21. doi:https://doi.org/10.1080/17455030.2019.1628320 (2019)
22. Abouelregal AE (2019) Two-temperature thermoelastic model without energy dissipation including higher order time-derivatives and two phase-lags. Materials Research Express 6(11):116535
23. Abouelregal AE (2020) On Green and Naghdi thermoelasticity model without energy dissipation with higher order time differential and phase-lags. Journal of Applied and Computational Mechanics 6(3):445–456
24. Abouelregal AE (2019) A novel generalized thermoelasticity with higher-order time-derivatives and three-phase lags. Multidiscip Model Mater Struct 16(4):689–711
25. Abouelregal AE (2020) Three-phase-lag thermoelastic heat conduction model with higher-order time-fractional derivatives. Indian J Phys 94:1949–1963
26. Abouelregal, A.E., Elhagary, M.A., Soleiman, A., Khalil, Generalized thermoelastic-diffusion model with higher-order fractional time-derivatives and four-phase-lags, Mechanics Based Design of Structures and Machines, (2020) https://doi.org/10.1080/15397734.2020.1730189, 1, 18
27. Amin, M.M., Abdel Allah Nasr, A.M., El-Bary, A.A., Abo-Dahab, S.M., Propagation of surface waves in generalized thermoelastic media under influence of magnetic field and rotation and its applications in engineering and geophysics, Mechanics Based Design of Structures and Machines, (2020) https://doi.org/10.1080/15397734.2020.1804934
28. Sharma DK, Thakur PC, Sarkar N (2020) Effect of dual-phase-lag model on free vibrations of isotropic homogenous nonlocal thermoelastic hollow sphere with voids. Mechanics Based Design of Structures and Machines:1–17. https://doi.org/10.1080/15397734.2020.1824792
29. Todorovic DM (2003) Plasma, thermal, and elastic waves in semiconductors. Rev Sci Instrum 74(582):1980
30. Sedighi HM (2014) Size-dependent dynamic pull-in instability of vibrating electrically actuated microbeams based on the strain gradient elasticity theory. Acta Astronautica 95:111–123
31. Brlić T, Rešković S, Jurković Z, Janeš G (2020) Mathematical modeling of the influence parameters during formation and propagation of the Lüders bands. Facta Universitatis, Series: Mechanical Engineering 18(4):595–610
32. Shariati A, Mohammad-Sedighi H, Żur KK, Habibi M, Safa M (2020) On the vibrations and stability of moving viscoelastic axially functionally graded nanobeams. Materials 13(7):1707
33. Pavlović IR, Pavlović R, Janevski G, Despenić N, Pajković V (2020) Dynamic behavior of two elastically connected nanobeams under a white noise process. Facta Universitatis, Series: Mechanical Engineering 18(2):219–227
34. Sedighi HM, Shirazi KH (2015) Dynamic pull-in instability of double-sided actuated nano-torsional switches. Acta Mechanica Solida Sinica 28(1):91–101
35. Qie N, Houa W-F, He J-H (2021) The fastest insight into the large amplitude vibration of a string. Reports in Mechanical Engineering 2(1):1–5
36. Ouakad HM, Sedighi HM (2016) Rippling effect on the structural response of electrostatically actuated single-walled carbon nanotube based NEMS actuators. International Journal of Non-Linear Mechanics 87:97–108
37. Ding W, Li Y, Dong W, Wei AL (2021) Constrainted least squares solution of Sylvester equation [J]. Mathematical Modelling and Control 1(2):112–120. https://doi.org/10.3934/mmc.2021009
38. Sedighi HM, Malikan M (2020) Stress-driven nonlocal elasticity for nonlinear vibration characteristics of carbon/boron-nitride hetero-nanotube subject to magneto-thermal environment. Phys Scr 95(5):055218
39. Sedighi HM, Daneshmand F (2014) Static and dynamic pull-in instability of multi-walled carbon nanotube probes by He's iteration perturbation method. J Mech Sci Technol 28(9):3459–3469
40. Shariati A, Mohammad-Sedighi H, Żur KK, Habibi M, Safa M (2020) On the vibrations and stability of moving viscoelastic axially functionally graded nanobeams. Materials 13(7):1707
41. Samaniego E, Anitescu C, Goswami S, Nguyen-Thanh VM, Guo H, Hamdia K, Rabczuk T (2020) An energy approach to the solution of partial differential equations in computational mechanics via machine learning: concepts, implementation and applications. Comput Methods Appl Mech Eng 362:112790
42. Rabczuk T, Ren H, Zhuang X (2019) A nonlocal operator method for partial differential equations with application to electromagnetic waveguide problem, CMC-computers. Materials & Continua 59(1):31–55
43. Cosmin Anitescu, Elena Atroshchenko, Naif Alajlan, Timon Rabczuk, Artificial Neural Network Methods for the Solution of Second Order Boundary Value Problems, CMC-Computers, Materials & Continua, Vol.59, No.1, pp. 345–359
44. Cheng JC, Zhang SY (2000) Normal mode expansion method for lasergenerated ultrasonic lamb waves in orthotropic thin plates. Appl Phys B Lasers Opt 70:57–63
45. Ghasemi H, Brighenti R, Zhuang X, Muthu J, Rabczuk T (2015) Optimum fiber content and distribution in fiber-reinforced solids using a reliability and NURBS based sequential optimization approach. Struct. Multidiscip. O. 51(1):99–112
46. Vu-Bac N, Lahmer T, Zhuang X, Nguyen-Thoi T, Rabczuk T (2016) A software framework for probabilistic sensitivity analysis for computationally expensive models. Adv Eng Softw 100:19–31
47. Vu-Bac N, Rafiee R, Zhuang X, Lahmer T, Rabczuk T (2015) Uncertainty quantification for multiscale modeling of polymer nanocomposites with correlated parameters. Comp Part B: Eng 68:446–464
48. Oliver Brand, Isabelle Dufour, Stephen M. Heinrich, and Fabien Josse, editors. Resonant MEMS. Advanced Micro and Nanosystems. Wiley-VCH, Weinheim, Germany, 2015
49. Li C, Gao S, Niu S, Liu H (2016) Study of intrinsic dissipation due to thermoelastic coupling in gyroscope resonators. Sensors 16(9):1445
50. Wang YZ, Liu D, Wang Q, Zhou JZ (2016) Thermoelastic behavior of elastic media with temperature-dependent properties under transient thermal shock. J Therm Stresses 39(4):460–473